Metals **2015**, *5*, 395-417; doi:10.3390/met5010395

OPEN ACCESS

metals

ISSN 2075-4701

www.mdpi.com/journal/metals/

Review

Temperature-Induced Liquid-Liquid Transition in Metallic Melts: A Brief Review on the New Physical Phenomenon

Fang-Qiu Zu

Liquid/Solid Metal Processing Institute, School of Materials Science & Engineering, Hefei University of Technology, Hefei 230009, China; E-Mail: fangqiuzu@hotmail.com; Tel.: +86-551-6290-5057; Fax: +86-551-6290-1362

Academic Editor: Enrique Louis

Received: 30 November 2014 / Accepted: 1 March 2015 / Published: 11 March 2015

Abstract: Understanding the nature of liquid structures and properties remains an open problem for many fundamental and applied fields. It is well known that there is no other defined phase line above *liquidus* (T_L) in phase diagrams of ordinary alloys. However, via resorts of internal friction, electric resistivity, thermal analysis, X-ray diffraction, solidification, *etc.*, the results of our research on lots of single- and multiple-component melts show a novel physical image: temperature induced liquid-liquid structure transition (TI-LLST) can occur above T_L. Moreover, the solidification behaviors and structures out of the melts that experienced TI-LLST are distinct from those out of the melts before TI-LLST. In this paper, some typical examples of TI-LLST and characteristic aspects of the TI-LLST are briefly reviewed, in which the main contents are limited in our own achievements, although other groups have also observed similar phenomena using different methods. In the sense of phenomenology, TI-LLST reported here is quite different from other recognized liquid transitions, *i.e.*, there are only a few convincing cases of liquid P, Si, C, H_2O, Al_2O_3-Y_2O_3, *etc.* in which the transition occurs, either induced by pressure or at a supercooled state and near *liquidus*.

Keywords: metals; alloys; liquid structures; properties of melts; solidification behaviors

1. Introduction

It is more and more clear that polymorphism in liquid states [1–3] is one of the most promising new fields, in which there are lots of puzzling phenomena and nature for experimentalists and theoreticians

to explore and to find their way to its applications, e.g., critical points between stable liquids and/or metastable ones [3–6]. Growing evidence suggests that the pressure-induced discontinuous phase changes might happen in some one-component liquids, e.g., SiO_2, H_2O, C, Si, Cs, Ga, Bi, I_2, and Se [1,6–12]. Such liquid state polyamorphism has been verified by an *in situ* X-ray study in liquid phosphorus, with an abrupt, pressure-induced structural change between two distinct forms [13]. Moreover, a temperature-induced phase transition was observed in the supercooled liquid system Al_2O_3-Y_2O_3 [14]. In addition, some liquid alloys, such as S-Te [15], Se-Te [16], and Cu-Ge [17], have been added to the systems in which the well-known conventional liquid phase separations can occur in the region near the *liquidus* with the chemical composition as the changing parameter. Because of the versatility of matter and the versatile complicated liquid structural nature, it is believed that novel phenomena and new knowledge will be uncovered as we probe liquid behaviors more deeply [6]. Accordingly, it is meaningful to explore if a temperature-induced structural change could discontinuously occur at ordinary pressure and at temperature far above melting point, or T_L, in single- or multiple-component liquids with a constant chemical composition

On the other side, liquid to solid transitions could be involved in most cases of the production or development of materials. It is a common phenomenon that structures and properties of many materials are related to the thermal history of their original melts, which has been intensively investigated in recent years. In developing semiconductors, the melt thermal history was shown to have a decisive influence on defect formation (twins) during crystallization and quality of ZnSe-based blue light-emitting laser diodes [18,19]. The microstructure of amorphous alloys is found to be much more homogeneous if precursor melts are much over-heated [20,21]. In order to refine solidified crystals, various techniques, like melt overheating and melt thermal treatment, have been explored and sometimes proved to be quite effective [22–26]. Although it is believed that the correlation between solidified microstructures and the melt thermal history would be attributed to different melt microstructures, the underlying nature and rules are unclear to date.

Unfortunately, knowledge about the liquid state has been much retarded in contrast to that of solid and gaseous states. On one hand, near *liquidus*, there is a general view that some kinds of residual micro-crystals still remain in the melts after fusion of crystal materials [1,27], *i.e.*, topological and/or chemical short-range ordering domains. On the other hand, near the liquid-gas critical temperature, the liquid structure of matter is hard to distinguish from its gaseous structure. Between the two typical cases, however, the change pattern of liquid structures and properties has been rarely concerned. Well what then is the underlying nature for the liquid-solid correlations and what rules are there for controlling solidification more effectively with less blindness by manipulating melt thermal history? Taking into account the abovementioned effects of liquids on solids and enlightened by liquid polymorphism [1–12,28,29], in the last ten years, our works suggest TI-LLST occurs well above the *liquidus* at ambient pressure in some ordinary alloys. In addition, we confirmed it is TI-LLST that decides liquid-solid effects at constant pressure and gives rise to significant alterations to solidification behaviors and structures.

A widely accepted conventional view about liquids is that the structures and properties change gradually with temperature or pressure [6,27]. It is worth noting that there is no other defined phase line above the *liquidus* in the phase diagrams of alloys. However, with the revised internal friction method,

resistivity, θ-θ X-ray diffraction, DSC, DTA, *etc.*, a new physical phenomenon, *i.e.*, TI-LLST, was experimentally observed in various kinds of alloy systems and pure elements, including:

- Simple eutectic systems, such as Pb-Sn, Sn-Bi, Pb-Sb, *etc.*
- Infinitely mutual soluble alloy, like Bi-Sb.
- Complex systems with peritectic reaction, e.g., Pb-Bi, In-Sn, Sn-Sb, Bi-Te, *etc*.
- Complex systems with compounds like Bi-In, Cu-Sn, Cu-Sb, In-Sb, Pb-In, *etc*.
- Pure elements like Sn, Bi, Sb, *etc.*
- Some multiple component systems.

Some typical examples of TI-LLST and its characteristic aspects are briefly reviewed as follows.

2. The Behaviors of Internal Friction with Changing Temperature in Some Liquid Alloys

Internal friction is a structure sensitive physical property and as a powerful technique widely used for studying crystal structures, defects and phase transitions in solids [30]. In our work, an improved torsion pendulum internal friction apparatus was, for the first time, used to study liquids, and it was verified to also be valid and sensitive to liquid structures [31–35]. The prior-prepared samples were re-melted and held for 60 min before internal friction experiments and shielded with 5N pure argon, and all experimental conditions and data collection were automatically controlled by a computer, for details of which please refer to [31–33].

Figure 1 shows the internal friction experiment results of the liquid samples with eutectic composition (PbSn61.9 wt%). Surprisingly, there is a notable peak in each Q^{-1}-T curves, around 670 ℃ at 2.5 ℃/min (Figure 1a) and 712 ℃ for 6.0 ℃/min (Figure 1b), hundreds of degrees above T_L (183 ℃). The peak position (T_P) moves to higher temperature when dT/dt rises, which is consistent with the kinetic nature of phase transitions. In order to detect what the Q^{-1}-T peak means for the Pb-Sn melt, the characteristics of the peak were analyzed. Figure 1 indicates clearly that T_P does not change with torsion frequencies (f), which resembles the internal friction feature in solid transitions. On the other hand, the magnitude of the peaks, *i.e.*, $Q_P^{-1} = Q^{-1}_{max} - Q^{-1}_{min}$, drops with increasing frequency (see Figure 1), but rises with the heating rate dT/dt; for example, at f = 0.5 Hz, Q_P^{-1} = 0.0125 for 2.5 ℃/min, while Q_P^{-1} = 0.0143 for 6 ℃/min. These features are perfectly in accordance with those of the first order phase transitions in solid internal friction (Delorme and Belko's Model: $Q_P^{-1} = A(dT/dt)/f$).

The internal friction characteristics in the eutectic Pb-Sn melt can be well repeated in other Pb-Sn melts with different compositions. However, peak position and magnitude change with Sn contents at the same heating rate and torsion frequency. The relevant data of different compositions for T_P at 2.5 ℃/min and 0.5 Hz are shown in the Pb-Sn phase diagram (Figure 2). We assume that, at a lower temperature, there are residual orders, *i.e.*, the phases L' (rich in Pb) and L" (rich in Sn), which are metastable and prone to homogenization. As temperature elevated, the atoms within the residual orders gain higher and higher energy. Once the critical temperature is reached, the energy is high enough to overcome the energy barrier so that the Pb-Pb and Sn-Sn atomic bonds in original phases are broken continuously. At the same time, the new Pb-Sn atomic bonds build up, which makes relatively homogeneous liquid phase (L) nucleates and they grow. That is, the phase transition

L'(Pb) + L''(Sn)→L(Pb-Sn) takes place. Similar patterns of internal friction with temperature were also observed in other liquid alloys, e.g., In-Sn80, In-Bi62 shown in Figures 3 and 4.

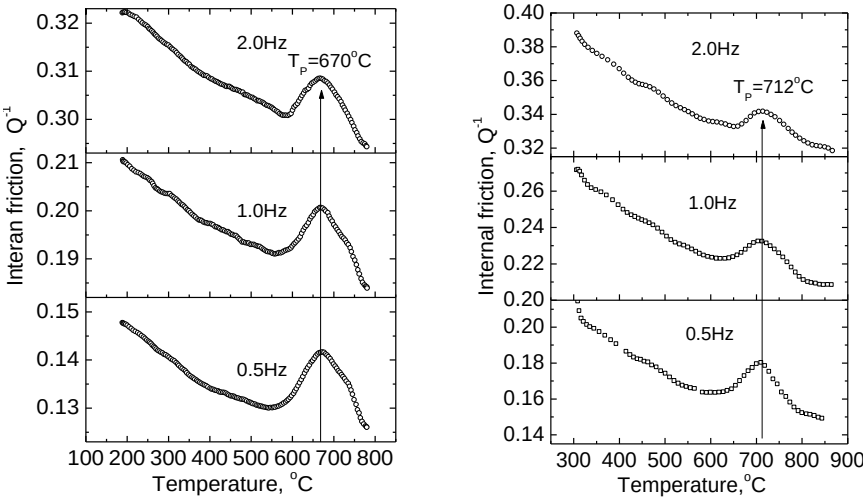

(**a**) d*T*/d*t* = 2.5 ℃/min (**b**) d*T*/d*t* = 6.0 ℃/min

Figure 1. Internal friction behavior of the melt Pb-Sn61.9.

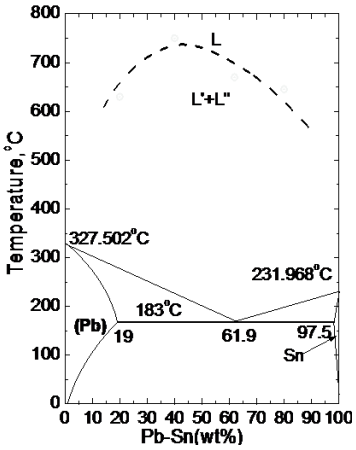

Figure 2. The temperature T_P of different compositions of Pb-Sn during heating process.

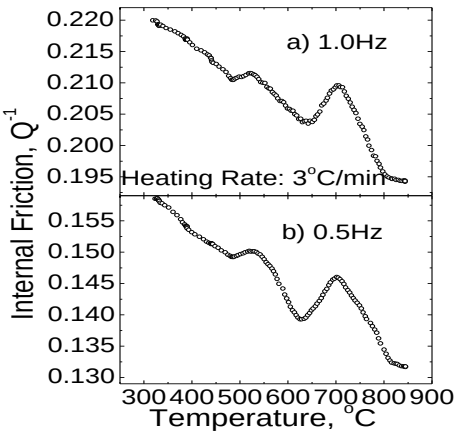

Figure 3. Q^{-1}-*T* behavior of the melt In-Sn80. (**a**) at frequency 1.0 Hz; (**b**) at frequency 0.5 Hz.

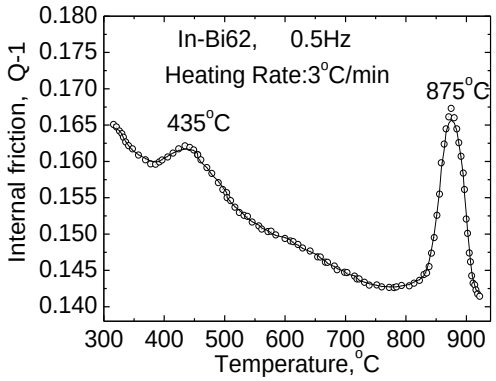

Figure 4. Q^{-1}-*T* behavior of the melt In-Bi62.

3. The Physical Characteristics of TI-LLST Confirmed by X-ray Diffraction

The results of internal friction experiments implied that TI-LLST occurred hundreds of degrees above T_L in some liquid alloys. However, it should be further confirmed if the results reflect a structure change and be found out what and how this happens during the process. To this goal, we performed X-ray diffraction measurements on In-Sn alloys. The reason for selecting In-Sn in the diffraction study is that the vapor pressure of both elements is quite low, so as not to stain the apparatus. The X-ray diffraction measurements were carried out using a θ-θ diffractometer with Mo-Kα-radiation; graphite monochromator; tantalum heater; corundum crucible; the sample chamber was evacuated beforehand to 10^{-6} mm Hg for inhibiting possibilities of contamination; and then filled with high pure Ar (4N) at 1.3 atm (see Refs [34,35] for detailed experiment procedures).

Based on the results of the diffraction experiment, through the use of correcting, normalization (Krogh-Moe-Norman Method) and inverse Fourier transform, we got the pair distribution functions g(*r*), shown in Figure 5, for the melt In-Sn80 at each temperature. Figure 6 shows the mean nearest neighbor distance (r_1) and the coordination number (N_1) derived from the pair distribution function g(*r*) at each temperature, respectively. For comparison, the internal friction pattern Q^{-1}-*T* of the melt In-Sn80 is also shown in the same figure, in which the prominent peak, around 700 ℃, was focused for selecting temperatures in X-ray diffraction measurements. Corresponding to the prominent peak of the internal friction in the curve Q^{-1}-*T*, as can be seen in Figure 6, a remarkable valley appears abnormally around about 700 ℃ for both r_1 and N_1, demonstrating evidently a discontinuous configuration reconstruction in the melt, while r_1 and N_1 vary only slightly with temperature before and after the valley. It should be noted that the values of both r_1 and N_1 after the valley are not much different from those before it (Figure 6). We assume that this is because the atomic radii of indium and tin are quite similar (the difference is less than 6%). However, the liquid structures before and after the configuration change are unlike. Before the change, there are the residual covalent bonds of solid tin in the melt, *i.e.*, the short-range ordering of tetrahedrons still exists. We suppose, in the melt, the atoms of indium do not distribute uniformly with those of tin, whereas they aggregate to some extent in microscopic zones surrounded by the domains composed mainly of tin atoms, showing a kind of metastable local ordering. During the transition, the residual covalent bonds are broken around 700 ℃, at the same time, new atomic bonds build up, with a relatively uniform melt forming. Since the melt is

mainly composed of tin, after the reconstruction, a reference Sn atom is surrounded by the nearest shell made up of about five or six atoms of tin and one or two atoms of indium (N_1 = 7.66 at 800 ℃).

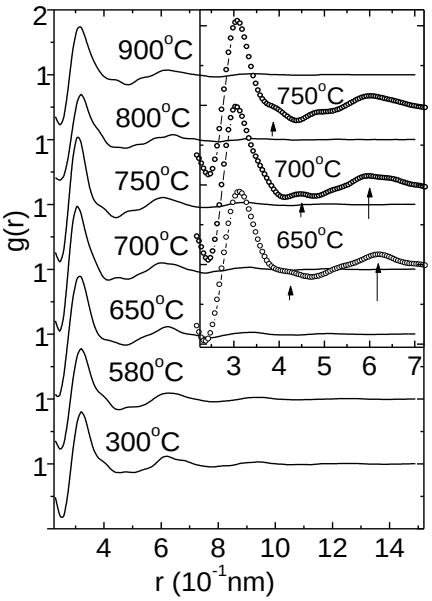

Figure 5. g(*r*) patterns of the melt In-Sn80 at each temperature.

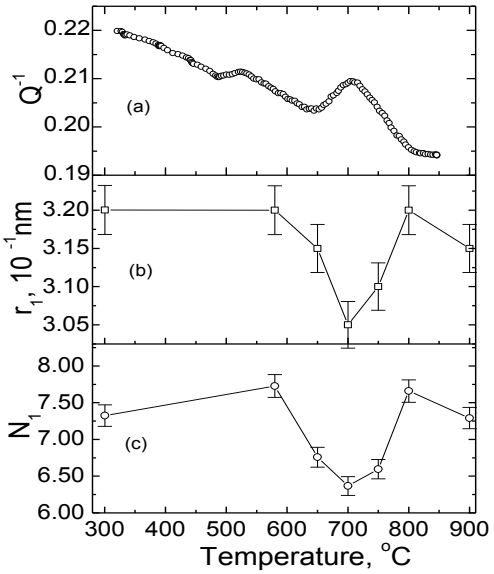

Figure 6. r_1, N_1 of In-Sn80 compared with Q^{-1}-T *versus* temperature. (**a**) Q^{-1} *versus* temperature; (**b**) r_1 *versus* temperature; (**c**) N_1 *versus* temperature.

In Figure 5, at about 700 ℃, there is a small hump (rather than a shoulder) between the first peak and the second one, and the latter leans to the left. According to the physical meaning of the pair correlation function g(*r*), the abnormal manners, compared with those at lower and higher temperatures, demonstrate that some atoms move amid the nearest atom shell and the next one around the reference atom, for example, the atoms of tin outwards and those of indium inwards. Of course, the same move takes place between further shells.

Using a semi-empirical approach [36], we got the functions of both r_C (the averaged ordering domain radius) and N_C (the atom number within the domains) *versus* temperature for the melt In-Sn80, as illustrated in Figure 7. From 750 ℃ to 800 ℃, r_C drops from 10.75 to 9.55, and N_C from 192 to 141, which indicate obviously that the ordering range becomes much smaller abruptly at the end of the structure change. In addition, Figure 7 also shows the parameter ζ (=r_C/r_1) whose pattern signifies that the ordering degree of the melt In-Sn80 decreases evidently along with the change.

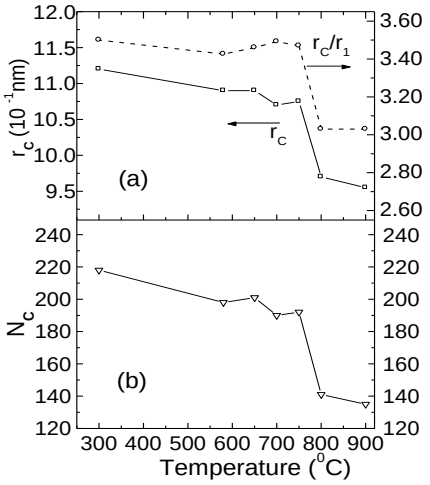

Figure 7. r_C, N_C and r_C/r_1 of In-Sn80 *versus* temperature. (**a**) r_C and r_C/r_1 *versus* temperature; (**b**) N_C *versus* temperature.

As is well known, r_1, N_1, r_C, N_C and r_C/r_1 are all important structural parameters for liquid matter, the peculiar behaviors confirm the occurrence of a discontinuous structural change in the melt In-Sn80. More importantly, they demonstrate explicitly the concrete physical meaning and characteristics of TI-LLST: during the liquid transition, through the adjustment of atomic bonds and the structural rearrangement, the size of short-range orders becomes smaller, and liquid structures are distinct from the original ones and reach a more homogeneous level. Similar phenomenon was also revealed in In-Sn20 melt, see Ref. [35].

4. Electrical Resistivity Behaviors of Liquid Alloys *versus* Temperature

In our investigations, the electrical resistivity method was used to study liquid alloys, too, and proved to be valid and sensitive to explore liquid structural changes because the results were in good accordance with those of other methods, such as internal friction, X-ray diffraction, DTA, and so on. In Figure 9, the abnormal behavior on resistivity-temperature curve (ρ-*T*) is in good accordance with the prominent peak of Q^{-1} and the valley of r_1, N_1 in Figure 6, although there is no sign of agreement with the small pre-peak of Q^{-1}, due to the difference of the methods. The detailed method of the electrical resistivity was demonstrated in Refs. [37–41].

The resistivity experiment results display abundant physical images of liquid matter in response to temperature. For examples, Figures 8–10 show some resistivity behaviors of several melts during heating and cooling processes, exhibiting different ρ-*T* patterns of liquid state and characteristics of TI-LLST. In some liquid alloys, two or more TI-LLST happen during heating process, e.g., Cu-Sn30

melt shown in Figure 8, while in some others only one TI-LLST happens, e.g., BiSb10 and Sn-Sb5 melts in Figures 10 and 11.

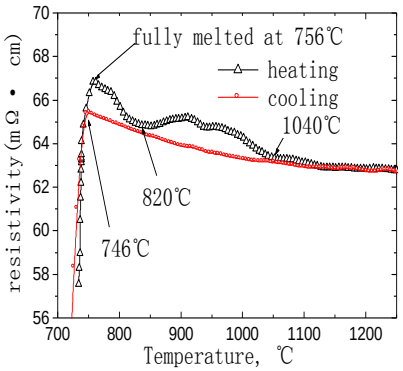

Figure 8. ρ-*T* curves of Cu-Sn30.

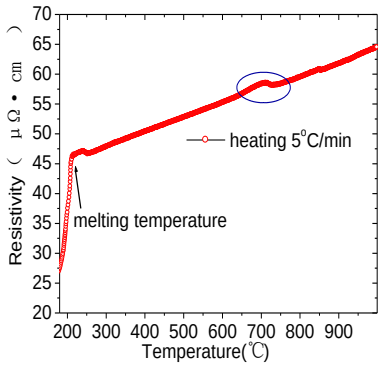

Figure 9. ρ-*T* curves of In-Sn80.

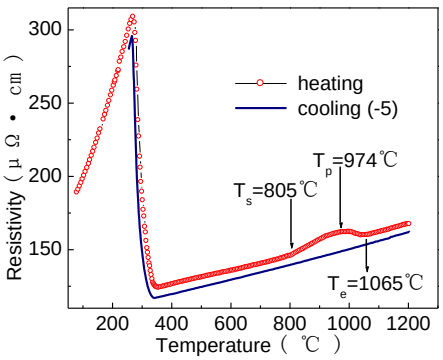

Figure 10. ρ-*T* curves of BiSb10.

Figure 12 shows the isothermal experiments of Pb-Sn61.9 holding at 888 K with the methods of resistivity and DTA (differential thermal analysis) [40]. During TI-LLST of Pb-Sn61.9, resistivity of the melt rises with a long "S" pattern (Figure 12). However, there are other resistivity patterns displaying TI-LLST during the heating process, such as a peak on ρ-*T* curve (Figures 9 and 10), a "Z" pattern (Figure 11), or a more complex pattern (Figure 8). In agreement with the ρ-*T* curve of Pb-Sn61.9 melt, there is an endothermic peak on the DTA curve, which suggests the entropy-driven mechanism and the discontinuous characteristic of TI-LLST.

Because of the sensitivity and the relative convenience of the resistivity method, up to now, the ρ-*T* behaviors of over one hundred liquid systems (alloys with different compositions or a single component) have been explored, whose results are listed in the table "Summary of TI-LLST suggested by the resistivity phenomena" as a Supplementary Material.

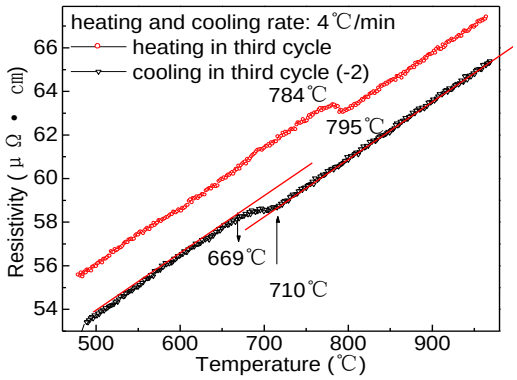

Figure 11. ρ-*T* curves of Sn-Sb5wt% melt.

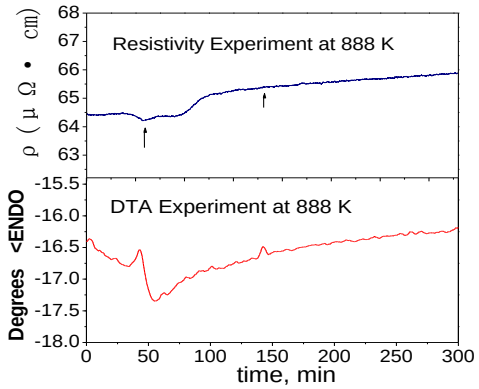

Figure 12. Isothermal experiments holding Pb-Sn61.9.

5. Primary Discussions about Temperature-Induced Liquid-Liquid Transition

Based on the abovementioned content, and the table "Summary of TI-LLST suggested by the resistivity phenomena", some aspects of TI-LLST are summarized as following.

5.1. If and How the Temperature-Induced Liquid-Liquid Transition Happens?

Because of the easy oxidation tendency of liquid metals and the various technical difficulties at high temperature, in our experiments, the temperature scope for the internal friction method (technically being only valid in heating process for liquids at present) is lower than 900 ℃, and that of the resistivity method is around 1200 ℃ (recently ameliorated up to 1400 ℃ or so) at most. So the alloys or pure components in our explorations are primarily limited in those whose *liquidus* or melting temperature and the oxidation tendency are as low as possible, specifically; chiefly limited in part of the IIIA-VIA elements (No. 49–52: In, Sn, Sb, Te and No. 82–83: Pb, Bi) and part of IB-IIB elements (No. 29–30: Cu, Zn and No. 47: Ag), and their alloys.

As can be seen in the Supplementary Materials, for all seven investigated pure elements, there is no sign of TI-LLST in liquid In, Pb, Te and Zn during the heating and cooling processes, while TI-LLST is suggested by repeated experiment results to occur in liquid Sn, Sb and Bi. Intriguingly, for the candidates of LLST in the supercooled liquid state, Poole *et al.* [1] prophesied that liquids with a locally open tetrahedral molecular structure are the most promising, such as Si, Ge, C, SiO_2, GeO_2, and H_2O. It has been confirmed with a marked shoulder at the right side of the first peak of g(*r*) and S(Q) that, in liquid Sn, Sb and Bi, there are residual covalent bonds of the solid with short-range ordering of tetrahedrons. The observations of TI-LLST here in liquid Sn, Sb and Bi widen Poole's theoretical prediction (liquids with open tetrahedral structure being the promising candidates of LLST) from the supercooled state to a much higher temperature scope, well above T_m. Another character of liquid Sn, Sb and Bi is that their ratio of Q_2/Q_1, Q_2 and Q_1 denoting the structure factor's position of second and first peaks, is much higher than that of the hard-sphere structure ($Q_2/Q_1 = 1.86$), being 1.96, 1.96 and 1.9, respectively [36].

For the investigated liquid alloy systems consisting of the abovementioned seven elements, except for Ag, Cu, Al, Si and Zr, phenomena of TI-LLST are observed in all the ternary liquid systems and most of the binary liquid systems, at least during the first heating process, while there is no sign of TI-LLST in some of the binary liquid systems. The exceptions include some Pb-Te melts with Te content higher than 75 weight percent (wt%), some Sn-Sb melts with Sb higher than 30 wt%, most of the In-Sb melts with Sb lower than 90 wt% and all the binary melts containing Zn. From the data accumulated to date, it is hard to conclude in what kinds of binary-component liquid systems TI-LLST can or cannot happen. We have attempted to understand the possibility of TI-LLST in binary melts from the viewpoint of the mixing enthalpies (ΔH_{mix}) indicating the inter-atomic force of unlike elements to some extent, but have come to no conclusion. We have also tried to understand from the kinds of constituent element in binary melts, but the only element that could be confirmed is Zn, with which alloys there is no TI-LLST. Indeed, Zn is a special metal element in respect of its liquid structure, whose first peak of structure factor S(Q) is quite asymmetrical, leaning towards the right, and is almost independent of temperature. Furthermore, the ratio of Q_2/Q_1 for Zn is the smallest (1.75) [36] in all the liquid metals, being considerably below the value of the hard-sphere structure ($Q_2/Q_1 = 1.86$).

The other fascinating fact is that, for the liquid systems in which TI-LLST is suggested to occur during the first heating process, for some melts there is no abnormality on the ρ-*T* curve during the cooling process, while for some others anomalies do occur during the first cooling process and even in further heating and cooling processes (in the second and third running). For the former cases, the TI-LLST is an irreversible liquid change, as shown in Figures 13a–c and 10. For the latter cases, the situations are relatively complicated. During the first cooling process, the abnormality of ρ-*T* is evidently corresponding to that or one of those during the first heating process for some melts. As can be seen in Figure 13d, for the melt Sn97Ag2.5Cu0.5, the second liquid change is reversible, while the first liquid change is irreversible. It should be noted that in a majority of the latter cases, it is hard to identify if the ρ-*T* abnormality on the first cooling marks the reversed process to that of the first heating, because the temperature difference between them is quite large, and the patterns of them are sometimes also distinct, as shown in Figure 13e,f. Intriguingly, as long as there is a sign of TI-LLST

on the first cooling, the reversibility of TI-LLST will show quite well in the second and third running, see also Figure 13e,f.

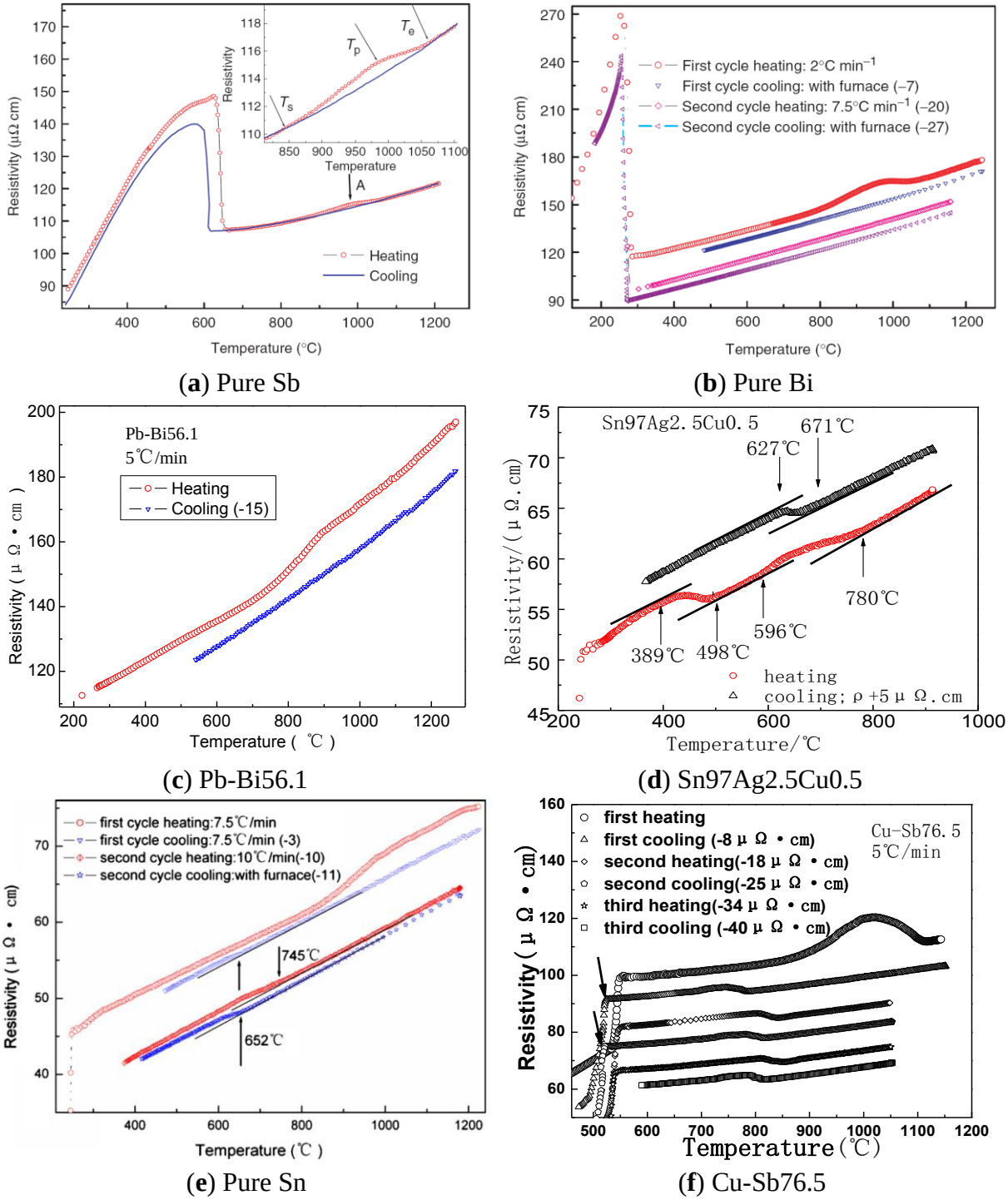

(**a**) Pure Sb (**b**) Pure Bi

(**c**) Pb-Bi56.1 (**d**) Sn97Ag2.5Cu0.5

(**e**) Pure Sn (**f**) Cu-Sb76.5

Figure 13. Is the TI-LLST reversible? Different behaviors of ρ-*T* in the first and further heating and cooling cycles.

5.2. What Happens During the Temperature-Induced Liquid-Liquid Transition?

With regard to what happens for TI-LLST during the first heating process, generally, we assume that it is a transition from an inhomogeneous liquid state to a more uniformed liquid state.

We think that there are topological short-range orders for pure liquids and the molten alloys with the positive or zero excess enthalpy, for example, different minor domains (rich in Pb and rich in Sn, as mentioned before) coexist heterogeneously in molten Pb-Sn alloys when temperature is not quite high. On the other hand, both the chemical and topological short-range orders exist in the liquid alloys with the negative excess enthalpy, for instance, both chemical short-range domains with the micro-structure similar to Ag_3Sn and the residual short-range ordering of tetrahedron of solid Sn coexist in molten AgSn alloys. Nevertheless, these minor domains dissipate and engender always with time and space as the fluctuation of energy, but they do not vanish with their statistical equilibrium structures, sizes and constituents, and change continuously with temperature elevated. However, as long as temperature reaches the critical scope, the inter-atomic bonds in original domains (the topological and/or chemical short-range orders) are broken, and the old domains (or minor phases) are reduced little by little, at the same time, new domains form with a relatively more uniformed liquid structure state.

The critical temperature range of TI-LLST depends on how strong the atomic bonds in the original domains are because the microstructures and the kinds of short-range orders are diversified in different pure liquids and molten alloys. For example, with the experimental results of scattering techniques, it was proposed that there are domains of both spherical close packing and layer lattice in the melts of Au, Ag, Pb, Tl and the alkali metals [27]. For liquid Sn, Bi, Sb, Ga and Si, shoulders appear at the right side of the first peak on the scattering curves after fusion, which is attributed to the short range ordering of tetrahedrons with the residual covalent bonds of solids in the liquids. It has been proved that there are regular icosahedrons and other clusters in liquid Pb [42] and many other simple liquids. Of course, the inter-atomic bonds in chemical short-range orders are also various, depending on liquid alloy systems and compositions. Generally, the stronger the inter-atomic bonds in old short-range orders, the higher the temperature range of TI-LLST. If there are species of short range orders with variety of bonding strength, which are able to change to others by TI-LLST, more than one liquid-liquid transitions will occur in different temperature ranges during the heating process, see the ρ-*T* patterns in Figures 8 and 13d. Typically, when the chemical short-range orders with strong bonds (*i.e.*, for the alloy with a large value of negative excess enthalpy) exist in the old liquid state, the temperature range of TI-LLST will be high. For example, for Cu-Zr alloy $\Delta H_{mix} = -23$ kJ/mol, the TI-LLSTs of the molten alloy Cu50Zr50 (T_L = 935 ℃) happen around 1230 ℃ and 1360 ℃, with two turning zones, see the table in Supplementary Materials.

As for the TI-LLST suggested by the anomalies of resistivity and other resorts during the first cooling process and even in further heating and cooling processes, based on their characteristics we assume that they could be divided into two kinds of TI-LLSTs. One is the reversed liquid-liquid transition corresponding to that during the first heating process. For instance, in liquid tin and some of its molten alloys, the domains of topological short-range ordering of tetrahedron of Sn dissipate during heating and recover during cooling. Similar cases can also happen for some chemical short-range orders in molten alloys with negative excess enthalpy. Another one is just such a kind of TI-LLST that is quite a distinct one from the TI-LLST during the first heating process because the newly generated short-range orders could not be recovered to those before the TI-LLST during the first heating. In this kind of TI-LLST, during the first cooling process and the further thermal runs, the micro-structures can be reversely transformed between different liquid states, both of which is dissimilar to that before the TI-LLST during the first heating.

5.3. Kinetics and Thermodynamics of Temperature-Induced Liquid-Liquid Transition

The investigation of kinetics and thermodynamics on TI-LLST reveal that the TI-LLST is accordance with kinetics characteristic and can be ranged into entropy driven type.

In terms of the ordering degree of a system, it is thermodynamically expressed by entropy. The pair correlation entropy S_2 (or called two-body excess entropy), defined by $S_2 = -2\pi\rho\int_0^\infty [g(r)\ln g(r) - h(r)]r^2 dr$ for amorphous systems, contributes at least 85% of the excess entropy S^E for liquids [43]. S^E signifies the difference between the thermodynamic entropy S^R of a real system and that of the equivalent ideal gas S^{ID}, *i.e.*, $S^E = S^R - S^{ID}$. Because entropy is always positive and the entropy of ideal gas S^{ID} larger than that of a real liquid S^R, the excess entropy S^E as well as the pair correlation entropy S_2 is negative forever for liquids. The smaller the absolute value of S_2 is, the less the ordering degree is in liquids. For convenience, we define the integration function of S_2 as $S(r) = -2\pi\rho[g(r)\ln g(r) - h(r)]r^2$. Here, $h(r) = g(r) - 1$, and is called the total pair distribution function, representing deviations from randomness, and ρ is the number density. It is reasonable to infer that the function $S(r)$ can give an intrinsic picture of the ordering degree. Figure 14 illustrates the patterns of the function $S(r)$ curves for the melt In-Sn20 as well as their integration results, the pair correlation entropy S_2, at different temperatures.

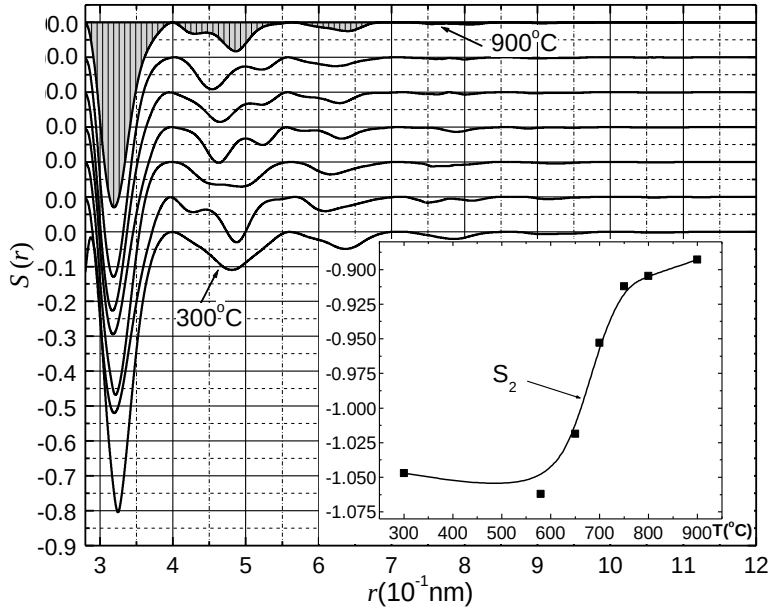

Figure 14. Patterns of the function $S(r)$ curves for the melt In-Sn20 as well as the pair correlation entropy S_2 (Inset) at different temperatures [35].

It is interesting to note that the function $S(r)$ is better than $g(r)$ in revealing the short-range ordering degree of liquid. From Figure 14, we clearly see that the magnitudes of the first, second, third and fourth inversed peaks of $S(r)$ decline quickly from 580 ℃ to 750 ℃. Up to high temperatures (including 750 ℃, 800 ℃, 900 ℃), the fourth inversed peak blurs out nearly completely, indicating the size of local short-range ordering reduces abruptly. Meanwhile, even more clearly, the absolute value of S_2, *i.e.*, the dark area surrounded by the curve $S(r)$, becomes smaller very fast from 580 ℃ to 750 ℃

(by about 15% between two liquid states), indicating a discontinuous drop of the ordering degree in the melt In-Sn20 during the configuration reconstruction. From the standpoint of thermodynamics, the steep change of entropy manifests the discontinuous characteristic of the L-L structure change. The entropy driven type characteristic of TI-LLST has also been verified by the thermal effect on DSC (differential scanning calorimetry) and DTA curves for lots of liquid systems, for instance, illustrated in Figures 12 and 15.

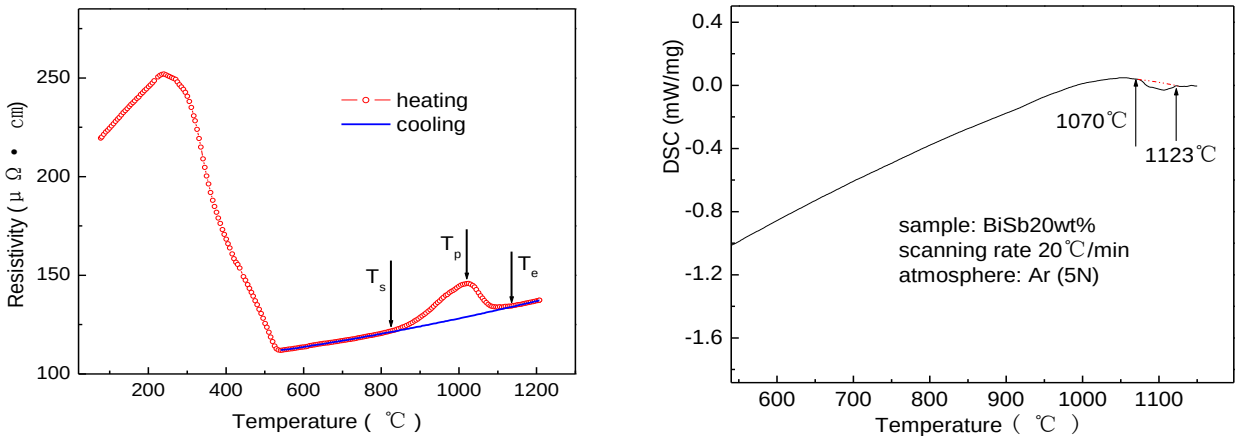

(**a**) Resistivity-temperature pattern (5 ℃/min) (**b**) DSC analysis in heating process (20 ℃/min)

Figure 15. Results of resistivity and DSC analysis for BiSb20 wt% alloy [41].

The kinetic behavior in TI-LLST process of those alloys has been investigated through continuous heating experiments and isothermal experiments. Using kinetic theory of phase transition, we found that the kinetic transition process is nucleation-growth type, and the nucleation rate is the dominant controlling factor of the TI-LLST process. There are two different kinds of transition modes for TI-LLST: Johnson-Mehl-Avrami transition mode and self-catalysis transition mode, whose microcosmic mechanism of the transition process has been discussed in Ref. [40]. Two characteristics of TI-LLST should be stressed here. At first, the transition speed of TI-LLST is much slower than that of normal solid state phase transitions, which can be seen from the large temperature width of TI-LLST, particularly for TI-LLST during the first heating process, normally between 100–200 ℃ or even wider at moderate speeds. Secondly, because both phases are liquid, the changes in energy, entropy, and density, *etc.* across the transition will be much smaller than those for the solid-solid, liquid-solid and liquid-gas transitions, which was also pointed out for liquid-liquid phase transitions in the supercooled liquid [1]. So it is not strange that the difference of S_2 before and after TI-LLST in Figure 14 is only 0.15, and that the thermal effect shown in Figure 15b is much less prominent than that of normal phase transitions. Based on the results of heating experiments, the apparent activation energy E_k of TI-LLST has been calculated using Kissinger equation for some liquid alloys [40,44]. E_k is the energy needed to overcome the energy barrier of the structure transition, and could reflect the difficulty level of TI-LLST of different alloy melts, for example InSn80 (1.60 ev) > InPb80 (1.45 ev) > PbSn61.9 (1.22 ev). Furthermore, compared with normal solid-state phase transition, the E_k value of TI-LLST is much smaller.

Based on the results of electronic transport properties and the calculated mean nearest neighbor atomic distance, the dependence of the density of electronic states $N(E_F)$ and its gradient value

d$N(E_F)$/dE on temperature were deduced with the help of Faber-Ziman theory, reflecting that the electronic structure of the melt at Fermi level also changes during the transition, e.g., illustrated in Figure 16 for In-Sn20 melt.

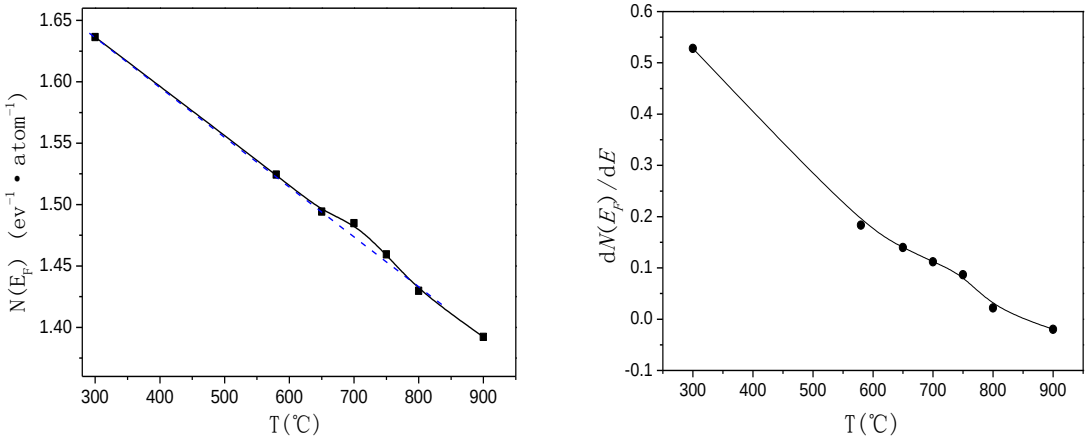

(**a**) $N(E_F)$-T of liquid InSn20 (**b**) d$N(E_F)$/dE of liquid InSn20

Figure 16. The density of state $N(E_F)$ and The d$N(E_F)$/dE of liquid InSn20 *versus* temperature [45].

Restricted to the paper space, the other specific characteristics of TI-LLST could not be illustrated here in detail; for further information please refers to Refs. [31–35,44–48].

It should be pointed out that, although the abovementioned results of TI-LLST are limited in the investigations of ourselves, the similar phenomena have been observed by other groups with different resorts like viscosity [49,50], density and sound velocity methods [51,52], as well as computer simulations [53,54]. For example, by high-resolution measurements of the density, the heat capacity and the static structure factor, scientists out of Israel, USA and France found that a temperature-driven liquid-liquid structural transformation takes place quite above *liquidus* of Bi [55]. Also, with high precision measurements, Greenberg *et al.* investigated the sound velocity-temperature behaviors in pure liquid tin and the results showed that at approximately 500 ℃ and 850 ℃ the data deviates by three times the experimental error from the linear fit [56]. By neutron diffraction and small-angle neutron scattering, a collaborative study on molten Al-Si alloys were carried out by University of Rouen (France), Ames Laboratory and Oak Ridge National Laboratory, and the results unambiguously show that for the eutectic Al-Si melt, the microstructure changes with increasing temperature in a partly reversible way, while for the hypereutectic (Al-Si20at%) melt, the change is almost completely irreversible [57]. A similar case was also found in a liquid Bi–Ga System [58]. Also, with the temperature dependence of the density, the viscosity and other properties of the Pd-18 at.% Si melt measured, Sivkov (Russia) *et al*. observed the existence of micro heterogeneities in the melt and a transformation of its microstructure at 1380-1430 K during a temperature cycle of heating and cooling [59]. In China, with experimental procedures like X-ray diffraction, internal friction, viscosity, resistivity, *etc.* as well as theoretical simulation methods, several other groups in Institute of Solid State Physics of Chinese Academy of Sciences [54,60,61], Shandong University [49,62,63], Jinan University [64] and Fudan University [53] observed lots of TI-LLST phenomena in liquid metals and alloys.

6. The Effects of TI-LLST on Solidification Behaviors and Structures

Based on the new physical phenomenon of TI-LLST, in recent years, the effects on solidification behaviors and structures resulted from different liquid structure states before and after TI-LLST have been explored. By comparison, for instance, two different melt treating procedures were used for carrying out solidification experiments, *i.e.*, the samples were melted at tempratures below and above the range of TI-LLST and held for one hour or longer, respectively. For the former, the melted samples were taken out of the furnace directly and cooled with the crucible in air (procedure A). For the latter, the melted samples were rapidly cooled to the same temperature as procedure A and held for 30 min, then taken out of the furnace and cooled with the crucible in air, too (procedure B), thus to obtain the same cooling condition as the procedure A. All samples were prepared from high pure elements (4~5 N) and shielded by flux, whose cooling curves *T-t* (Temperature-time) of solidification were automatically recorded by a system with the error less than 0.1 ℃. The effects of TI-LLST on solidification behaviors and structures are briefly summarized as follows.

Illustratively, the results of Bi-Sb 10 alloy are shown in Figures 17–19.

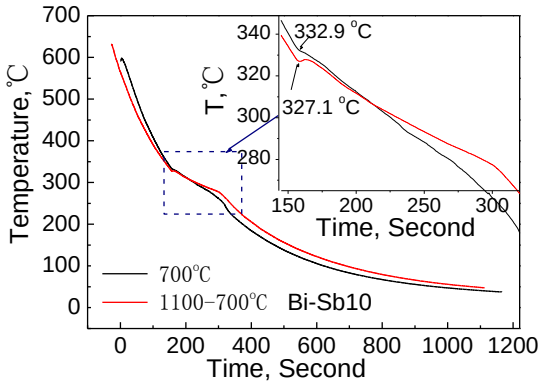

Figure 17. Bi-Sb10 T-t curves of different melts.

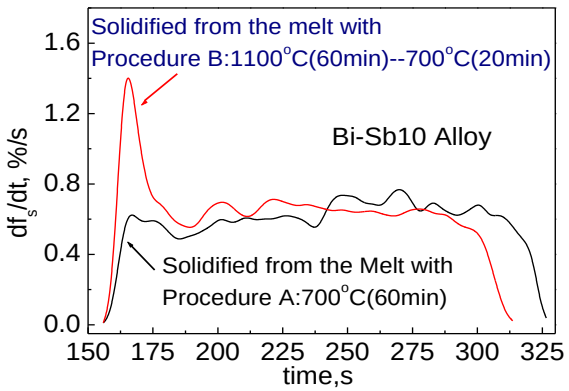

Figure 18. Solidification rate obtained by NTA method.

At first, it is evident that, for the liquid alloys in which TI-LLST occurs and is not reversible, the under-cooling of the samples treated with procedure B is larger than that of those with procedure A, the normal enlargement of the under-cooling being about 5–20 ℃. As shown in Figure 17 for Bi-Sb10 alloy [65], as the T_L of Bi-Sb10 is 346 ℃, the nucleation under-cooling increases from 13.1 ℃ of the

procedure A to 18.9 ℃ of the procedure B. Figure 18 shows the solidification rate curves of Bi-Sb10, df_S/dt-t, obtained by Newton Thermal Analysis (NTA) method [66], here df_S/dt indicates the solid fraction f_S increased in unit time. According to Kurz' theory [67], the altitude of the first peak on df_S/dt-t curve betokens the level of nucleation rate, the apparently enhanced peak of df_S/dt-t for the sample with procedure B signifies a quite higher nucleation rate. The enlarged under-cooling brings about the higher nucleation rates and evident refined solidification structures, which can be seen in Figure 19.

Similar effects of refined solidification structures were also observed in dozens of different alloys, such as Babbitt alloys (Sn-Cu-Sb), piston alloys (hyper-eutectic Al-Si), Pb-free solder alloys, thermoelectric alloys (Bi-Te/Sb), *etc*. As shown in Figure 20, for example, in hyper-eutectic Al-Si20 wt% alloy, which can be used for pistons of engines and other wear-resisting parts, the crystals of primary silicon are much refined with a more uniformed distribution with the procedure B process.

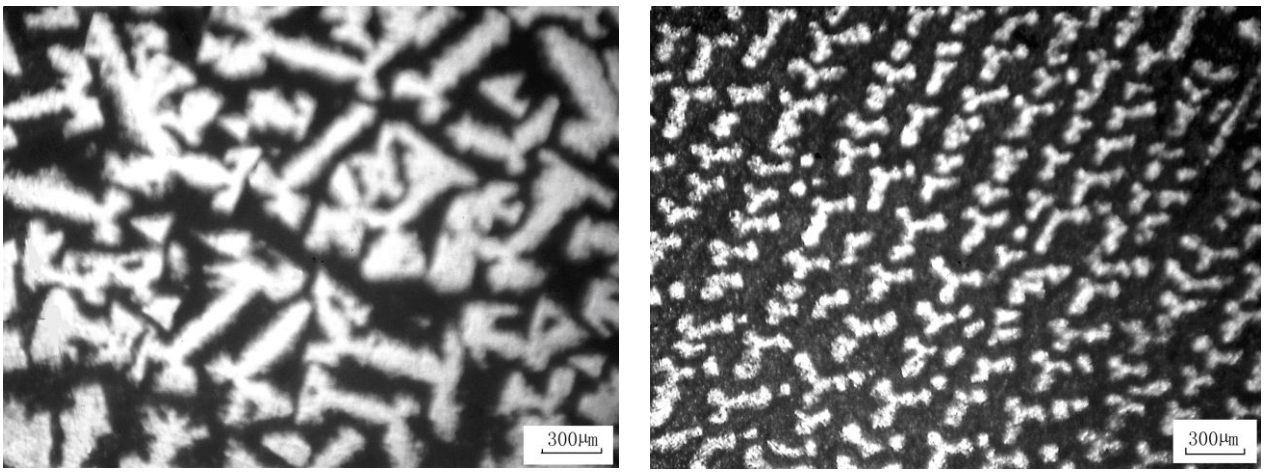

(**a**) procedure A: 700 ℃ for 60 min (**b**) procedure B: 1100 ℃ for 60 min + 700 ℃ for 30 min

Figure 19. Solidified structures of the Bi-Sb10 (wt %) alloy from different liquid states.

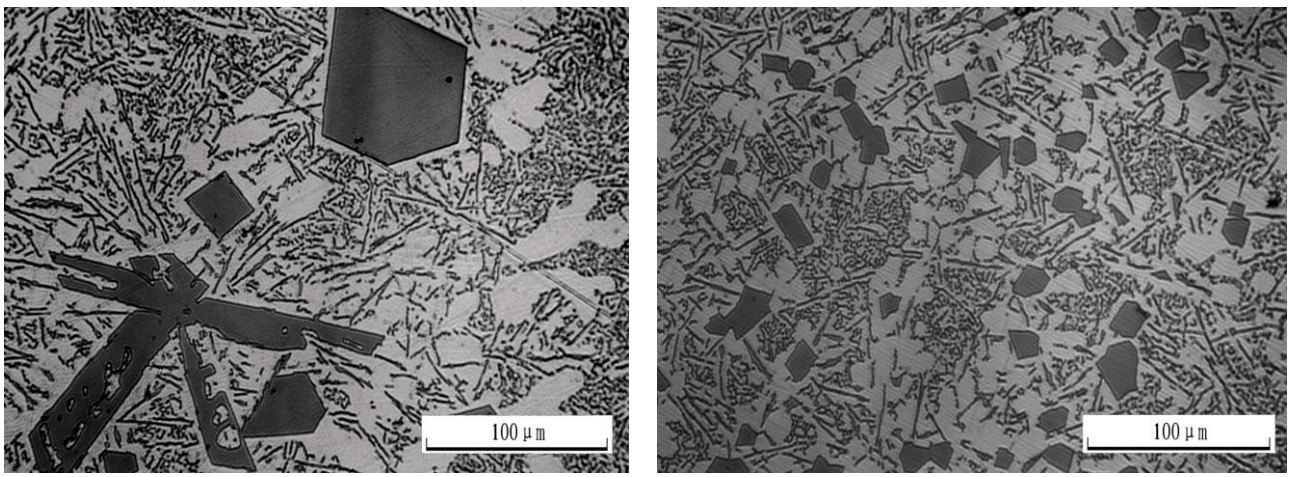

(**a**) procedure A: 760 ℃ for 90 min

(**b**) procedure B: mixing the melt at 1150 ℃ with the melt at 660 ℃ (1:1), and then hold in the furnace at 760 ℃ for 5 min

Figure 20. Solidified structures of the Al-Si20 (wt%) alloy from different liquid states.

Because of the changes of solidified structures of alloys with TI-LLST, some of the engineering properties can be evidently improved. For instance, the wettability (Figure 21) and the shear strength (Figure 22) of the Pb-free solder Sn-3.5Ag-*x*Bi/Cu joint are ameliorated.

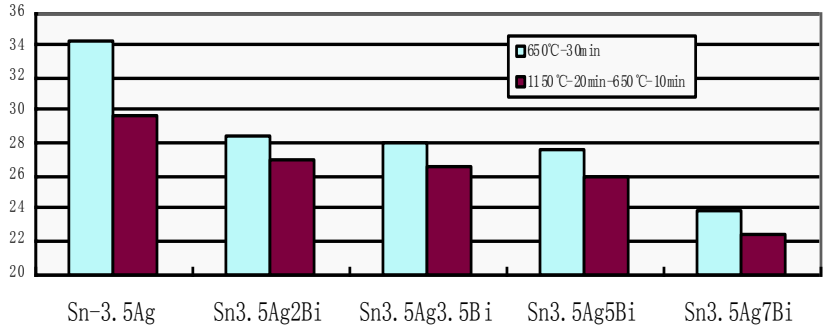

Figure 21. The effect of melt state on the wettability (wetting angle θ°) of Pb-free solder Sn-3.5Ag-*x*Bi/Cu joint [68].

Figure 22. The effect of melt state on the shear strength (MPa) of Sn-3.5Ag-*x*Bi/Cu joint [68].

On the other hand, the effective partition coefficient $K_E(C_S/C_L)$ becomes smaller because the melt experienced TI-LLST, thus leading to changes of the solute redistribution process during solidification and the morphology of the solidified structures.

It should be pointed out that the liquid thermal history has no influence on solidification because it results in no different liquid state if a liquid system without TI-LLST, *i.e.*, for the alloy Sn-Sb42 without TI-LLST detected, no apparent difference of solidified structures can be observed between lower and higher melt processing temperature. Even though liquid structure transition could occur, it is not always effectual to change solidification behaviors by melt thermal resorts if TI-LLST is reversible in the system. Whether it is effective to control solidification depends on how to manipulate the melt thermal history for curbing the structural reverse process, too.

7. Summary

1. As opposed to the conventional view of liquids that liquid structures and properties change gradually with temperature, with different resorts, temperature induced discontinuous liquid structure transitions were observed to occur in some alloy systems and pure elements.
2. Results show that the averaged ordering domain radius (r_C) and the atom number within the domains (N_C) drop abruptly during TI-LLST, and the ordering degree parameter $\zeta(=r_C/r_1)$ decreases evidently

along with the liquid change. Analyses of the results suggest the entropy-driven mechanism for TI-LLST. The temperature dependence of density of electronic states $N(E_F)$ and its gradient value $dN(E_F)/dE$ reflects that the electronic structure of the melt at Fermi level also changes during TI-LLST.

3. The kinetic process of TI-LLST belongs to nucleation-growth type, and the nucleation rate is the dominant controlling factor of the TI-LLST process. There are two different kinds of transition modes for TI-LLST: Johnson-Mehl-Avrami transition mode and self-catalysis transition mode. Through the adjustment of atomic bonds, the size of short-range orders becomes smaller, and liquid structures are distinct from the original ones and reach a more homogeneous level.
4. If an irreversible TI-LLST occurs, it brings about different liquid states and results in enlarged undercooling and an altered solute redistribution process during solidification, which gives rise to refined grains and improved configurations. However, in a system without TI-LLST, the liquid thermal history has no influence on solidification owing to no difference in liquid state. Furthermore, if TI-LLST is reversible, then effects of the melt manipulation are dependent on whether the reverse process could be prevented after TI-LLST.
5. Because of the present technical and theoretical limits, and the restricted scope of liquids already investigated to date, there is a long way to go to understand the nature of TI-LLST. However, the already disclosed abundant phenomena of TI-LLST open a new window for experimentalists and theoreticians to recognize polymorphism in liquid states, to explore it further and to find their way to its applications.

Acknowledgments

The author is indebted to all the colleagues and students who partly contributed to the relevant contents in this paper, and to Zhu Z.G. and Jiang J.Z. for their support and valuable discussions. The works have been financially supported by the National Natural Science Foundation of China Grant No.50571033 and No.50371024, the National Basic Research Program of China (973 Program) (No.2012CB825702), the key project of Chinese Ministry of Education No.104106, the Natural Science Foundation of Anhui Province No.070414178, and the Grant Project of Hefei University of Technology RC-2002-01.

Author Contributions

The author is the principal researcher and the director of all the above listed projects except for No.2012CB825702, and the writer of this paper.

Conflicts of Interest

The author declares no conflict of interest.

References

1. Poole, P.H.; Grande, T.; Angell, C.A.; McMillan, P.F. Polymorphic phase transitions in liquids and glasses. *Science* **1997**, *275*, 322–323.

2. Rao, K.R. Phase transitions in liquids. *Curr. Sci.* **2001**, *80*, 1098–1100.
3. Yarger, J.L.; Wolf, G.H. Polymorphism in Liquids. *Science* **2004**, *306*, 220–221.
4. Kurita, R.; Tanaka, H. Critical-like phenomena associated with liquid-liquid transition in a molecular liquid. *Science* **2004**, *306*, 845–848.
5. White, J.A. Multiple critical points for square-well potential with repulsive shoulder. *Physica A* **2005**, *346*, 347–371.
6. McMillan, P. Jumping between liquid states. *Nature* **2000**, *403*, 151–152.
7. Saika-Voivod, I.; Sciortino, F.; Chester, P.H. Computer simulations of liquid silica: Equation of state of liquid-liquid transition. *Phys. Rev. E* **2001**, *63*, 011202.
8. Lacks, D.J. First-order amorphous-amorphous transformation in silica. *Phys. Rev. Lett.* **2000**, *84*, 2881–2884.
9. Mishima, O.; Stanley, H.E. Decompresion-induced melting of ice IV and the liquid-liquid transition in water. *Nature* **1998**, *392*, 164–168.
10. Koga, K.; Tanaka, H.; Zeng, X.C. First-order transition in confined water between high-density liquid and low-density amorphous phases. *Nature* **2000**, *408*, 564–567.
11. Soper, A.K.; Ricci, M.A. Structures of high-density and low-density water. *Phys. Rev. Lett.* **2000**, *84*, 2881–2884.
12. Glosli, J.N.; Ree, F.H. Liquid-liquid phase transition in carbon. *Phys. Rev. Lett.* **1999**, *82*, 4659–4662.
13. Katayama, Y.; Mizutani, T.; Utsumi, W.; Shimomura, O.; Yamakata, M.; Funakoshi, K. A first-order liquid-liquid phase transition in phosphorous. *Nature* **2000**, *403*, 170–172.
14. Aasland, S.; MaMillan, P.F. Density-driven liquid-liquid phase separation in the system Al_2O_3-Y_2O_3. *Nature* **1994**, *369*, 633–636.
15. Coulet, M.-V.; Bergman, C.; Bellissent, R.; Bichara, C. Local order and phase separation in sulphur–tellurium melts: A neutron scattering study. *J. Non-Crystal. Solids* **1999**, *250–252*, 463–467.
16. Tsuchiya, Y.; Kakinuma, F.; Bergman, C. Structural changes and concentration fluctuations in the liquid Se-Te system. *J. Non-Crystal. Solids* **1996**, *205–207*, 143–146.
17. Kaban, I.; Halm, T.; Honyer, W. Structure of molten copper-germanium alloys. *J. Non-Crystal. Solids* **2001**, *288*, 96–102.
18. Rudolph, P.; Schaefer, N.; Fukuda, T. Crystal growth of ZnSe from the melt. *Mater. Sci. Eng. R Rep.* **1995**, *15*, 85–133.
19. Wang, J.F.; Omino, A.; Isshiki, M. Bridgman growth of twin-free ZnSe single crystals. *Mater. Sci. Eng. B* **2001**, *83*, 185–191.
20. Dahlborg, U.; Calvo-Dahlborg, M. Influence of the production conditions on the structure and the microstructure of metallic glasses studied by neutron scattering techniques. *Mater. Sci. Eng. A* **2000**, *283*, 153–163.
21. Popel, P.S.; Sidorov, V.E. Microheterogeneity of liquid metallic solutions and its influence on the structure and properties of rapidly quenched alloys. *Mater. Sci. Eng. A* **1997**, *226–228*, 237–244.
22. Enisz, M.; Kristof-Mako, E.; Oravetz, D. Phase transformation in doped Y-Ba-Cu-O superconductors obtained by different melt processing techniques. *J. Eur. Ceram. Soc.* **2007**, *27*, 1105–1111.
23. Koh, H.J.; Rudolph, P.; Schaefer, N.; Umestsu, K.; Fukuda, T. The effect of various thermal treatments on supercooling of Pb-Te melts. *Mater. Sci. Eng. B* **1995**, *34*, 199–203.

24. Li, P.; Nikitin, V.I.; Kandalova, E.G.; Nikitin, K.V. Effect of melt overheating, cooling and solidification rates on Al–16wt.%Si alloy structure. *Mater. Sci. Eng. A* **2002**, *332*, 371–374.
25. Sidorov, V.; Popel, P.; Calvo-Dahlborg, M.; Dahlborg, U.; Manov, V. Heat treatment of iron based melts before quenching. *Mater. Sci. Eng. A* **2001**, *304–306*, 480–486.
26. Wang, J.; He, S.H.; Sun, B.D.; Guo, Q.X.; Nishio, M. Grain refinement of Al–Si alloy (A356) by melt thermal treatment. *J. Mater. Process. Technol.* **2003**, *141*, 29–34.
27. Ubbelohde, A.R. *The Molten State of Matter: Melting and Crystal Structure*; Wiley: New York, NY, USA, 1978.
28. Franzese, G.; Malescio, G.; Skibinsky, A.; Buldyrev, S.V.; Stanley, H.E. Generic mechanism for generating a liquid-liquid phase transition. *Nature* **2001**, *409*, 692–695.
29. Tanaka, H. General view of a liquid-liquid phase transition. *Phys. Rev. E* **2000**, *62*, 6968–6976.
30. Nowic, A.S.; Berry, B.S. *Anelastic Relaxation in Crystalline Solids*; Academic Press: New York, NY, USA, 1972.
31. Zhu, Z.G.; Zu, F.Q.; Guo, L.J.; Zhang, B. Internal friction method: suitable also for structural changes of liquids. *Mater. Sci. Eng. A* **2004**, *370*, 427–430.
32. Zu, F.Q.; Zhu, Z.G.; Guo, L.J.; Zhang, B.; Shui, J.P.; Liu, C.S. Liquid-liquid transition in Pb-Sn melts. *Phys. Rev. B* **2001**, *64*, 180203.
33. Zu, F.Q.; Zhu, Z.G.; Zhang, B.; Feng, Y.; Shui, J.P. Post-melting anomaly of Pb-Bi melts observed by internal friction technique. *J. Phys.* **2001**, *13*, 11435–11441.
34. Zu, F.Q.; Zhu, Z.G.; Guo, L.J.; Qin, X.B.; Yang, H.; Shan, W.J. Observation of an anomalous discontinuous liquid-structural change with temperature. *Phys. Rev. Lett.* **2002**, *89*, 125505.
35. Zu, F.Q.; Li, X.F.; Guo, L.J.; Yang, H.; Qin, X.B.; Zhu, Z.G. Temperature dependence of liquid structures in In–Sn20: Diffraction experimental evidence. *Phys. Lett. A* **2004**, *324*, 472–478.
36. Waseda, Y. *The Structure of Non-Crystalline Materials*; McGraw-Hill: New York, NY, USA, 1980.
37. Li, X.F.; Zu, F.Q.; Ding, H.F.; Yu, J.; Liu, L.J.; Li, Q.; Xi, Y. Anomalous change of electrical resistivity with temperature in liquid Pb-Sn alloys. *Phys. B Condens. Matter* **2005**, *358*, 126–131.
38. Xi, Y.; Zu, F.Q.; Li, X.F.; Yu, J.; Liu, L.J.; Li, Q.; Chen, Z.H. High-temperature abnormal behavior of resistivities for Bi-In melts. *Phys. Lett.* **2004**, *329*, 221–225.
39. Li, Q.; Zu, F.Q.; Li, X.F.; Xi, Y. The electrical resistivity of liquid Pb-Bi alloy. *Morden Phys. Lett. B* **2006**, *20*, 151–158.
40. Chen, Z.H.; Zu, F.Q.; Li, X.F.; Yu, J.; Xi, Y.; Shen, R.R. Temperature-induced liquid-liquid transition process in eutectic Pb–Sn melt explored from kinetic viewpoint. *J. Phys. Condens. Matter* **2007**, *19*, 116106.
41. Li, X.F.; Zu, F.Q.; Ding, H.F.; Yu, J.; Liu, L.J.; Xi, Y. High-temperature liquid-liquid structure transition in liquid Sn-Bi alloys: Experimental evidence by electrical resistivity method. *Phys. Lett. A* **2006**, *354*, 325–329.
42. Spaepen, F. Five-fold symmetry in liquids. *Nature* **2000**, *408*, 781–785.
43. Baranyai, A.; Evans, D.J. Direct entropy calculation from computer simulation of liquids. *Phys. Rev. A* **1989**, *40*, 3817–3822.
44. Zu, F.Q.; Chen, Z.H.; Zou, L. Kinetics of liquid–structure change of In–Sn and In–Pb melt. *Phys. Chem. Liquids* **2008**, *46*, 433–441.

45. Zou, L.; Zu, F.Q.; Li, X.F.; Chen, Z.H.; Chen, H.S.; Guo, L.L.; Sun, Q.Q. Electronic transport properties of liquid InSn20 alloy. *Phase Transit.* **2008**, *81*, 889–896.
46. Zu, F.Q.; Shen, R.R.; Xi, Y. Electrical resistivity of liquid Sn-Sb alloy. *J. Phys. Condens. Matter* **2006**, *18*, 2817–2823.
47. Zu, F.Q.; Xi, Y.; Shen, R.R.; Li, X.F.; Zhang, Y.; Chen, Z.H. Effects of compound formation on liquid structure in Cu-Sn melts as a function of temperature. *Phys. Chem. Liquids* **2006**, *44*, 543–550.
48. Shen, R.R.; Zu, F.Q.; Li, Q.; Xi, Y.; Li, X.F.; Ding, G.H.; Liu, H.M. Study on temperature dependence of resistivity in liquid In-Sn alloy. *Phys. Scr.* **2006**, *73*, 184–187.
49. Wang, L.; Bian, X.F.; Liu, J.T. Discontinuous structural phase transition of liquid metal and alloys. *Phys. Lett. A* **2004**, *326*, 429–435.
50. Sun, C.; Geng, H.R. Viscous and structural behaviors of molten In–Sn alloys. *Mater. Charact.* **2005**, *55*, 383–387.
51. Plevachuk, Y.; Sklyarchuk, V.; Yakymovych, A.; Willers, B.; Eckert, S. Electronic properties and viscosity of liquid Pb–Sn alloys. *J. Alloys Compd.* **2005**, *394*, 63–68.
52. Nasch, P.; Manghnani, M.M.; Secco, R.A. Anomalous behavior of sound velocity and attenuation in liquid Fe-Ni-S. *Science* **1997**, *227*, 219–221.
53. Ji, M.; Gong, X.G. *Ab Initio* molecular dynamics simulation on temperature-dependent properties of Al–Si liquid alloy. *J. Phys. Condens. Matter* **2004**, *16*, 2507–2514.
54. Liu, C.S.; Li, G.X.; Liang, Y.F.; Wu, A.Q. Quantitative analysis based on the pair distribution function for understanding the anomalous liquid-structure change in In20Sn80. *Phys. Rev. B* **2005**, *71*, 4204–4210.
55. Greenberg, Y.; Yahel, E.; Caspi, E.N.; Benmore, C.; Beuneu, B.; Dariel, M.P.; Makov, G. Evidence for a temperature-driven structural transformation in liquid bismuth. *Europhys. Lett.* **2009**, *86*, 36004.
56. Greenberg, Y.; Yahel, E.; Ganor, M.; Hevroni, R.; Korover, I.; Dariel, M.P.; Makov, G. High precision measurements of the temperature dependence of the sound velocity in selected liquid metals. *J. Non-Crystal. Solids* **2008**, *354*, 4094–4100.
57. Dahlborg, U.; Besser, M.; Calvo-Dahlborg, M.; Cuello, G.; Dewhurst, C.D.; Kramer, M.J.; Morris, J.R.; Sordelet, D.J. Structure of molten Al-Si alloys. *J. Non-Crystal. Solids* **2007**, *353*, 3005–3010.
58. Khairulin, R.A.; Stankus, S.V.; Sorokin, A.L. Determination of the two-melt phase boundary and study of the binary diffusion in liquid Bi–Ga system with a miscibility gap. *J. Non-Crystal. Solids* **2007**, *297*, 120–130.
59. Sivkov, G.; Yagodin, D.; Kofanov, S.; Gornov, O.; Volodin, S.; Popel, P.; Sidorov, V.; Bao, C.; Calvo-Dahlborg, M.; Dahlborg, U.; *et al*. Physical properties of the liquid Pd-18 at.% Si alloy. *J. Non-Crystal. Solids* **2007**, *353*, 3274–3728.
60. Wu, A.Q.; Guo, L.J.; Liu, C.S. Structural characteristics of liquid Sn. *Chin. Phys. Lett.* **2005**, *22*, 1991–1993.
61. Wang, Y.B.; Zhao, G.; Liu, C.S.; Zhu, Z.G. *Ab initio* molecular dynamics simulations on the structural change of liquid eutectic alloy Si15Te85 from 673 to 1373 K. *Phys. B Condens. Matter* **2010**, *405*, 785–792.

62. Zhou, C.; Hu, L.; Sun, Q.; Qin, J.; Bian, X.; Yue, Y. Indication of liquid-liquid phase transition in CuZr-based melts. *Appl. Phys. Lett.* **2013**, *103*, 171904.
63. Wang, Y.Q.; Wu, Y.Q.; Liu, J.T.; Bian, X.F. Discontinuous structural phase transition behaviour in multiple component alloy melts. *Chin. Phys. Lett.* **2006**, *23*, 2513–2515.
64. Wang, Z.M.; Geng, H.R.; Zhou, G.R.; Guo, Z.Q.; Teng, X.Y. Metastable microheterogeneity in liquid monotectic Bi-Ga alloys. *Int. J. Cast Metals Res.* **2011**, *24*, 65–69.
65. Li, X.F.; Zu, F.Q.; Yu, J.; Zhou, B. Effect of liquid-liquid transition on solidification of Bi-Sb10 wt% alloy. *Phase Transit.* **2008**, *81*, 43–50.
66. Stefanescu, D.M.; Upadhya, G.; Bandyopadhyay, D. Heat Transfer-Solidification Kinetics Modeling of Solidification of Castings. *Metall. Mater. Trans. A* **1990**, *21*, 997–1005.
67. Kurz, W.; Fisher, D.J. *Fundamentals of Solidification*; Trans Tech Publications: Zurich, Switzerland, 1998; p. 28.
68. Li, X.Y. Research on Effects of Melt State of SnAgBi Lead-Free Solders on Solidification Microstructure and Welding Joint Reliability. Ph.D. Thesis, Hefei University of Technology, Hefei, China, June 2013.